Atomic and molecular adsorption on RhMn alloy surface: A first principles study

Xiufang Ma,[1,2] Huiqiu Deng,[1,a)] Ming-Mei Yang,[2] and Wei-Xue Li[2,b)]
[1]*Department of Applied Physics, Hunan University, Changsha 410082, China*
[2]*State Key Laboratory of Catalysis, Dalian Institute of Chemical Physics, Chinese Academy of Sciences, Dalian 116023, China*

(Received 27 September 2008; accepted 19 November 2008; published online 31 December 2008)

Density functional theory calculations have been employed to study the effects of alloy on energetics and preferential adsorption sites of atomic (H, C, N, O, S), molecular (N_2, NO, CO), and radical (CH_3, OH) adsorption on RhMn(111) alloy surface, and underlying electronic and structural reasons have been mapped out. We find that though Mn is energetically favorable to stay in the subsurface region, the RhMn surface alloy may be developed via the segregation induced by strong interaction between oxygen-containing species and Mn. Independent of adsorbates (not including O and OH), the interactions between these species and Rh atoms are preferential, and enhanced in general due to the ligand effects induced by Mn nearby. In contrast, oxygen-containing species (atomic oxygen and hydroxyl) prefer to coordinate with Mn atom due to the significant hybridization between oxygen and Mn, a manifestation of the ensemble effects. The order of the binding energies on RhMn alloy surface from the least to the most strongly bound is $N_2 < CH_3 < CO < NO < H < OH < O < N < S < C$, which is also found on Rh(111) surface, due to the distinct reactivity of these species overwhelming the ligand/ensemble effects present in surface alloy. The implication of the modification of the adsorption energy, site preferences, and their relative stability on RhMn alloy surface, on the syngas ($CO+H_2$) selective conversion, are discussed. © *2008 American Institute of Physics*. [DOI: 10.1063/1.3046691]

I. INTRODUCTION

Catalytic conversion of syngas (carbon monoxide and hydrogen) from reforming of natural gas and coal to hydrocarbon (Fishcher-Tropsch synthesis) and oxygenates attracts extensive efforts due to the limited resources of petroleum available on the planet. Among them, rhodium (Rh) is a unique catalyst for its higher selectivity on the production of C_2 oxygen-containing compounds, such as acetic acid, ethanol, and acetaldehyde.[1,2] Moreover, it is found that the catalytic activity and/or selectivity can be improved further by introducing promoters in Rh catalysts.[3–8] Manganese (Mn) receives particular concern due to its ability to increase the activity and selectivity for the production of C_2 oxygenates.[9–13] Recent study shows further that the addition of Mn is essential for the formation of ethanol and acetic acid with selectivity larger than 50%.[14] Rhodium also plays a critical role in three-way catalyst for simultaneous conversion of nitride oxide, carbon oxide, and unburned hydrocarbon and partial oxidation of methane.[15]

The importance of Rh catalysts on catalytic reactions mentioned above calls for the detail microscopic study, particularly on the adsorption of relevant molecules in terms of the energetics and site preferences on Rh catalysts as well as the effects of Mn added. It has been well documented in literature that the alloy surfaces often lead to superior activity and selectivity because of the modification of the relative stability of the reactants due to the possible ligand effects, strain effects, and ensemble effects induced by the second elements.[16–25] Particularly, the ability of alloy surfaces with multiple adsorption sites and reaction centers are thought to be crucial for the catalysts with desired selectivity and free of poisons.[26–28]

In this work, an extensive set of atomic (H, C, N, O, S), molecular (N_2, CO, NO), and radical (OH and CH_3) species on RhMn(111) surface alloy is studied by density functional theory (DFT) calculations in terms of their energetics, adsorption sites, and structures, supplemented with detailed electronic structural analysis. These species are selected because they are relevant for the catalytic reactions mentioned in above. Additionally, Mavrikakis *et al.* studied the adsorption of the similar set of species on Rh(111) using DFT in the past,[29] which can be compared with the present work to illustrate the effects of the alloy. In that work, a thorough overview of available experiment data is presented with references therein.

Our DFT study indicates that RhMn(111) surface alloy presents distinct reactivity with respect to Rh(111) surface. Independent of adsorbates (not including O and OH), the interactions between these species and Rh atoms are preferential and enhanced, in general, due to the ligand effects induced by Mn nearby. In contrast, oxygen-containing species (atomic oxygen and hydroxyl) prefer to coordinate with Mn atom due to the significant hybridization between oxygen and Mn, a manifestation of the ensemble effects. The order of the binding energies on RhMn alloy surface from

a)Electronic mail: hqdeng@gmail.com.
b)Electronic mail: wxli@dicp.ac.cn.

the least to the most strongly bound is $N_2 < CH_3 < CO < NO < H < OH < O < N < S < C$, which is also found on Rh(111) surface, due to the distinct reactivity of these species overwhelming the ligand/ensemble effects present in surface alloy. The implication of the modification of the adsorption energy, site preferences, and their relative stability on RhMn alloy surface, on the syngas ($CO+H_2$) selective conversion, is discussed. The remainer of this paper is organized as follows. The calculation methods are described in Sec. II. Section III covers the main computational results. The underlying electronic mechanisms and implications are discussed in Sec. IV. Finally, conclusions are presented in Sec. V.

II. COMPUTATION METHODS

All calculations were carried out using the plane wave code DACAPO.[30] Ionic cores were described by ultrasoft pseudopotentials (USPPs),[31] and the Kohn-Sham one-electron valence states were expanded in plane waves basis with kinetic energy of 340 eV and electronic density cutoff of 400 eV. The self-consistent electronic density was determined by iterative diagonalization of the Kohn-Sham Hamiltonian with Fermi population of the Kohn-Sham states (k_BT=0.1 eV) and Puly mixing of the resulting electronic density. The exchange-correlation energy and potential were described by generalized gradient approximation (GGA) in the form of revised Perdew-Burke-Ernzerhof (RPBE), which gives better description of the adsorption energies than other functionals.[30] Whenever Mn was involved, spin-polarized calculations were performed without statement otherwise. The calculated lattice constant for bulk Rh is 3.84 Å, which agrees well with the experiments (3.80 Å),[32] has been used in the present work. A five layer Rh(111)-(2×2) slab (corresponding surface coverage of 0.25 ML), periodically repeated in a supercell geometry with seven equivalent layers of vacuum between any two successive metal slabs, was used to simulate the surfaces. The surface Brillouin zone was sampled by $(6\times6\times1)$ Monkhorst-Pack grid.[33] Adsorptions were allowed only on one side of the exposed surfaces, and the electrostatic potential was corrected by adding a dipole layer in the vacuum, accordingly.[34] The chemisorbed species and the atoms in the top two metal layers were fully relaxed till the residual forces was less than 0.02 eV/Å, while the remaining atoms were fixed to their bulk truncated positions. Spin-polarization calculations for isolated species were carried out in a $(12.2\times12.1\times12$ Å$^3)$ unit cell with single K point.

The RhMn(111) alloy surface was simulated by substitution of a quarter of surface Rh atoms with Mn atoms. A number of adsorption sites (top, bridge, fcc, and hcp hollow sites) on RhMn(111) and Rh(111) surfaces were considered, and but only energetically favorable sites were presented in the present work without statement otherwise. With the presence of Mn, adsorbed species may coordinate either with surface Rh or Mn atoms only, or coordinate with both Rh and Mn atoms at same time. To differentiate these, a convention was defined as follows. For example, fccRh represents the adsorption at threefold fcc hollow site coordinated with three surface Rh atoms, while fccRhMn for the adsorption at the fcc follow site coordinated with (two) surface Rh atoms and (one) surface Mn atom. For adsorption at the top site, topRh and topMn mean the adsorption at the top of Rh and Mn atoms with single coordination, respectively. The adsorption sites considered are shown schematically in Fig. 1.

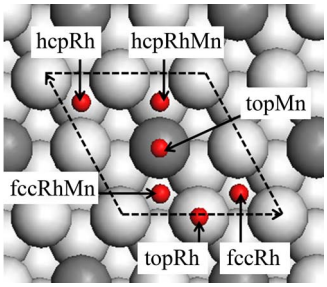

FIG. 1. (Color online) The schematic representation (top view) of the RhMn(111) surface alloy. White balls represent Rh, deep gray balls for Mn, and small red balls for possible adsorption sites. The (2×2) unit cell is indicated by dashed lines.

In the present work, the binding energy E_b was calculated to be the energy gain of the adsorption with respect to the clean substrates and corresponding species in the gas phase. Here, a negative (positive) value indicates that the adsorption is exothermic (endothermic). For comparison, the binding energies for adsorption on Rh(111) surface were calculated to illustrate the alloy effects. Our test calculations show that the computational setups are well converged. Increasing the plane wave cutoff up to 500 eV, the relative change between two adsorption systems is less than 20 meV, which has no effect on the conclusion derived from the present.

III. RESULTS

A. RhMn surface alloy

To alloy Mn with Rh(111) surface, we note that adsorption of Mn adatom on Rh(111) is unfavorable. For example, adsorption of Mn adatom at coverage of 0.25 ML with respect to clean Rh(111) substrate and optimized fcc bulk Mn is endothermic with energy of 0.06 eV for hcp Mn, and 0.12 eV for fcc Mn, respectively. Instead, substitution of surface Rh atoms is found to be energetically favorable. We find that it costs 1.26 eV to generate Rh vacancy, but the occupation of the Rh vacancy by a bulk fcc Mn atom releases the energy by 2.09 eV in a given (2×2) unit cell. As a result, overall energetics by forming RhMn surface alloy is exothermic with energy of −0.83 eV. Further calculations show that substitution of subsurface Rh atom is lowered further to −1.02 eV, but the energy for Mn incorporation into the bulk raises to −0.74 eV. These calculations indicate that rather than staying in surface and bulk Rh layers, Mn tends to stay in the subsurface region. However, as shown in the following calculations, the significant stronger interaction between Mn and oxygen-containing species (such as atomic oxygen and hydroxyl group), which are typically presented under reactive conditions, would induce Mn segregation from the subsurface region, and RhMn surface alloy will be eventually developed. We therefore focus our study on RhMn surface alloy in the present work.

TABLE I. Calculated binding energies (E_b) of atomic species considered on RhMn(111) and Rh (111) surfaces. The reference zero corresponds to gas phase atoms at infinite separation from the slab. ΔE_b represents the difference of binding energy between different adsorption sites on RhMn(111) surface. Energy unit is given in eV.

		RhMn(111)		Rh(111)	
	Site	E_b	ΔE_b	E_b (present)	E_b (Ref. 29)
H	fccRhMn	−2.70	0.09		
	fccRh	−2.79		−2.69	−2.62
O	fccRhMn	−4.97	−0.13		
	fccRh	−4.84		−4.64	−4.31
N	hcpRhMn	−4.85	0.30		
	hcpRh	−5.15		−4.88	−4.87
S	fccRhMn	−4.87	0.42		
	fccRh	−5.29		−5.04	−4.95
C	hcpRhMn	−6.46	0.68		
	hcpRh	−7.14		−6.84	−6.65

TABLE II. Main structural parameters (Å) and adsorption induced variations of work function ($\Delta\phi$ in eV) for various atomic species considered on RhMn(111). d_{A-Rh} and d_{A-Mn} represents the bond length between atom and applicable surface Rh or Mn atoms. Calculated work function of clean RhMn(111) surface is 4.80 eV.

	Site	d_{A-Rh}	d_{A-Mn}	$\Delta\phi$
H	fccRh	1.87		0.05
	fccRhMn	1.80	2.07	0.10
O	fccRh	2.01		0.50
	fccRhMn	2.03	1.88	0.55
N	hcpRh	1.90		0.36
	hcpRhMn	1.91	1.87	0.49
S	fccRh	2.29		0.20
	fccRhMn	2.30	2.30	0.40
C	hcpRh	1.89		0.44
	hcpRhMn	1.86	2.01	0.52

B. Atomic adsorptions

Atomic adsorption, such as H, C, N, O, and S at different sites, as indicated schematically in Fig. 1, was calculated and described here. We find that for atomic adsorption, all of them prefer to adsorb exclusively on the highly coordinated threefold hollow sites, and only the adsorption at energetically favorable fcc and/or hcp hollow sites is presented in Table I and discussed in the following, correspondingly. For comparison, the adsorption on Rh(111) from the present and previous calculations is given. Important structural parameters and adsorption induced variation of work function are shown in Table II.

Among atomic adsorption on RhMn(111) surface, atomic hydrogen is the least strongly bound atom with a binding energy of −2.79 eV (with respect to atomic H in gas phase) at the fccRh site. For H adsorption at fccRhMn site, where H coordinates with two Rh atoms and one Mn atom, calculated binding energy is −2.70 eV (Table I). H adsorption energy at threefold hollow sites on clean Rh(111) surface at same coverage (0.25 ML) is −2.69 eV, which agrees well with previous calculation (−2.62 eV) (Ref. 29) and experimental measurement (−2.66 eV).[35,36] These indicate that H prefers to adsorb at threefold Rh atoms with Mn nearby. The stronger bonding at fccRh site can be justified further from the smaller bond length between H and Rh atoms than Mn, as listed in Table II.

The next least strongly bound atom is oxygen. Different from H adsorption, the preferential adsorption site for atomic oxygen is fccRhMn with binding energy of −4.97 eV (Table I). If oxygen coordinates with Rh atoms only (fccRh), calculated adsorption energy is −4.84 eV, which is 0.13 eV (ΔE_b in Table I) higher than oxygen coordinating partially with Mn. The origin of the stronger interaction between O and Mn will be discussed later. Oxygen would induce Mn agglomeration in surface and form Mn domain, correspondingly. The interaction between oxygen and Mn may increase further due to the increase coordination number between oxygen and Mn domain. The strong interaction between oxygen and Mn compensates the segregation energy (less than 0.19 eV) of Mn from the subsurface and bulk, and RhMn surface alloy is developed. As will be shown in the following, not only oxygen but also hydroxyl group may induce Mn segregation from subsurface region.

Compared to oxygen adsorption, the binding between atomic nitrogen and RhMn surfaces increases further, as clearly seen in Table I. In contrast to the adsorption of atomic oxygen, which prefers to coordinate with Mn (fccRhMn), atomic nitrogen tends to bond with threefold Rh atoms with binding energy of −5.15 eV (hcpRh). When one N–Rh bond is substituted by one N–Mn bond (hcpRhMn), the interaction between N and substrates underneath is destabilized by 0.30 eV, and the calculated binding energy is −4.85 eV, accordingly. For sulfur and carbon atomic adsorption, energetically preferential sites are found to be fccRh site (−5.29 eV) and hcpRh (−7.14 eV), respectively, which are significantly stronger than atomic nitrogen. Same as N, we find that S and C atoms prefer to bind with Rh rather than Mn. When S and C atoms are coordinated with Mn, the binding energies decrease by 0.42 and 0.68 eV (ΔE_b in Table I), respectively. The large difference of calculated binding energies for S and C between fcc/hcpRh and fcc/hcpMn sites indicates that both of them prefer to coordinate exclusively with Rh atoms rather than Mn, a clear site selectivity (ensemble effects) for RhMn surface alloy.

The preferences of the coordination and site are corroborated further with respect to the variation of the bond length between adsorbed atomic species and metal atoms coordinated. For example, for carbon adsorption on RhMn alloy surface, the binding energy for carbon adsorption at hcpRhMn site is 0.68 eV weaker than the adsorption at hcpRh. In line with this, the bond length of C–Mn bond (2.01 Å) is longer than that of C–Rh bond (1.86 Å), as shown in Table II. This means comparable weaker interaction between carbon and Mn atoms than the interaction with Rh. This becomes evident by taking into account the fact that the Wigner-Seitz radius of corresponding metal solid for Mn

TABLE III. Calculated binding energies (E_b) of molecule and radical species on RhMn(111) and Rh (111) surfaces. All optimized configurations are perpendicular to the surface. The reference zero corresponds to the gas phase species at infinite separation from the slab. ΔE_b represents the adsorption energy difference between different adsorption sites on RhMn(111) surface. Energy unit is given in eV.

		RhMn (111)		Rh(111)		
	Site	E_b	ΔE_b	E_b (present)	E_b (previous)	Expt.
N_2	topMn	0.12	0.53	−0.35	−0.34[a]	−0.36[b]
	topRh	−0.14				
CH_3	topMn	−1.18	0.29	−1.47	−1.49[a],	
	topRh	−1.47			−1.42[c]	
CO	hcpRh	−1.87		−1.75	−1.68[a]	−1.65[d]
	hcpRhMn	Unstable				
NO	hcpRhMn	−1.94	0.29	−2.05	−1.83[a]	−1.48[d]
	hcpRh	−2.23				
OH	fccRhMn	−2.83	−0.24	−2.51	−2.30[a]	
	fccRh	−2.59				

[a]Reference 29.
[b]Reference 38.
[c]Reference 39.
[d]Reference 44.

(1.43 Å) is smaller than that of Rh (1.49 Å).[37] For S and N, the destabilization energies (ΔE_b given in Table I) induced by coordination with one Mn atom decrease to 0.42 eV (S) and 0.30 eV (N), compared to 0.68 eV for carbon. Correspondingly, the bond lengths between S–Mn (2.30 Å) become close to that of S–Rh bond (2.29–2.30 Å) (Table II), while the N–Mn bond (1.87 Å) is even smaller than N–Rh bond (1.90–1.91 Å). For O adsorption, since the binding at fccRhMn site is stronger than that of fccRh, one would expect that the O–Mn bond length is shorter than that of O–Rh bond, as indeed found in our calculations, 1.88 Å for the previous one and 2.03 Å for the latter one. The fact of larger difference between O–Mn and O–Rh bond (0.15 Å) than that of Wigner-Seitz radius between Mn and Rh (0.06 Å) indicates further the stronger O–Mn binding than that of O–Rh. The origin of the site preference (ensemble effects) will be discussed later on the electronic structure analysis. In Table II, the adsorption induced variations of work function are given. It is interesting to note that all of atomic species considered induce exclusively increase of the work function (positive $\Delta\phi$), which means a net charge transfer from the substrates to adsorbed species.

C. Molecular and radical adsorptions

N_2, CO, NO, and CH_3, OH adsorptions on RhMn(111) and Rh(111) surfaces are described in this section. Same as above, we report the results in the order from the least to the strongest bound sequence. The calculated binding energies at preferential adsorption sites are given in Table III, and the main structural parameters and the adsorption induced variations of work function are listed in Table IV. In Fig. 2, favorable adsorption configurations are indicated.

Among molecules and radicals discussed, we find that N_2 is the least strong bound molecule with binding energy of

TABLE IV. Main structural parameters (Å) and adsorption induced variations of work function ($\Delta\phi$ in eV) for molecule and radical species considered on RhMn(111). d_{A-Rh} and d_{A-Mn} represent the bond length between adsorbed species and applicable surface Rh/Mn atoms. Calculated work function of clean RhMn(111) surface is 4.80 eV.

	Site	d_{A-Rh}	d_{A-Mn}	$\Delta\phi$
N_2	topRh	1.92		0.50
	topMn		2.05	−0.04
CH_3	topRh	2.11		−0.21
	topMn		2.04	−0.16
CO	hcpRh	2.09		1.42
NO	hcpRh	2.04		0.99
	hcpRhMn	2.05	1.99	1.10
OH	fccRh	2.19		−1.58
	fccRhMn	2.23	2.04	−1.50

−0.41 eV at favorable topRh site (Table III), and N_2 molecule is found to be perpendicular to the surface (Fig. 2). Adsorption at topMn site is endothermic with binding energy of 0.12 eV. The dramatic difference of binding energies between topRh and topMn sites indicates that N_2 molecules will coordinate exclusively with surface Rh atoms. For comparison, we calculate N_2 adsorption on top site of Rh(111) surface, and find that the binding is slightly weaker than the adsorption on RhMn(111) surface alloy. Calculated binding energy with value of −0.35 eV on Rh(111) agrees well with experimental measurement (−0.36 eV) based on thermal desorption spectroscopy experiments[38] and previous DFT calculations (−0.34 eV).[29]

Compared to N_2 adsorption, methyl radical (CH_3) is found to bind much stronger with the substrate. Our calculations show that methyl radical prefers to adsorb at RhMn(111) topRh site with binding energy of −1.47 eV, and the optimized configuration is plotted schematically in Fig. 2. Methyl adsorption at RhMn(111) topMn site is found to be less favorable with binding energy of −1.18 eV. The binding energy for the radical adsorption on Rh(111) is calculated to be −1.47 eV, which agrees well with previous DFT calculations.[29,39]

For CO adsorption on RhMn(111) and Rh(111) surfaces, only adsorption at hcp sites is considered to illustrate the effect of alloy, though CO adsorption at top sites at low coverages is found to be favorable adsorption sites.[40] Calcu-

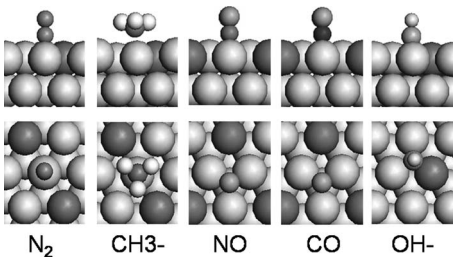

FIG. 2. Schematic representation of preferential adsorption sites for various molecules and radicals on RhMn(111) surface alloy. (Upper panel, side view; lower panel, top view.)

lated binding energy for CO adsorption at hcpRh site is −1.87 eV. A strong repulsion between CO and Mn is found. Actually, our calculation indicates that CO adsorption with coordinated Mn is not stable. For CO adsorption on Rh(111) surface, calculated binding energy at hcp site is −1.75 eV, which is slightly higher than the adsorption on the RhMn(111) surface. On both surfaces, we find that adsorbed CO at hollow sites is perpendicular to the surface, which agrees well with experimental findings[41] and previous DFT calculations.[29,42]

The next stronger bound molecule is NO. Calculated binding energy for NO adsorption at favorable hcpRh site of RhMn surface is −2.23 eV, and −1.94 eV for adsorption at unfavorable hcpRhMn site (Table III), respectively. Optimized NO is found to be perpendicular to the surfaces. A pronounced destabilization (~0.30 eV) by replacing one NO–Rh bond with NO–Mn bond can be seen. For NO adsorption on Rh(111), we find that the hcp hollow site is the energetically favorable adsorption site, as found by experiments.[43] Corresponding binding energy is −2.05 eV, which is slightly higher than NO adsorption on threefold Rh atoms with Mn nearby, a manifestation of the ligand effect induced by Mn nearby. The large difference of the binding energy between calculations and experiments[44] may come from uncertainty for the latter one as discussed in Ref. 29.

The last species with the strongest binding considered in this work is the hydroxyl group. The hydroxyl group is found to prefer to adsorb at threefold fcc hollow site. Calculated binding energies for OH adsorption at fccRh and fccRhMn sites are −2.59 and −2.83 eV, respectively, and calculated ΔE_b is −0.24 eV. The coordination preference for OH to Mn atom is in contrast to those of molecules and radicals discussed above, but the same with atomic oxygen adsorption on RhMn(111). Larger ΔE_b than segregation energy of Mn (0.19 eV) means that the hydroxyl group may induce Mn segregation from the subsurface region and RhMn surface alloy is developed, as found for atomic oxygen. Compared to OH adsorption on Rh(111) with binding energy of −2.51 eV, slightly larger OH adsorption at fccRh in RhMn(111) surface (−2.59 eV) indicates again the ligand effects induced by Mn nearby.

Geometrical parameters in terms of bond length between adsorbed molecular/radical species and coordinated surface metal atoms are given in Table IV. For N_2 adsorption, the bond length between N_2 and Rh (topRh) is 1.92 Å, which is significantly smaller than the adsorption at topMn (2.05 Å), despite of the smaller Wigner-Seitz radius of Mn (0.06 Å) than Rh. This is in line with the weaker binding between N_2 and Mn from the calculations. A similar case can be found for CO. For NO and CH_3 adsorption, where the destabilizations induced by coordination with Mn are less pronounced (ΔE_b=0.29 eV for NO and CH_3), the smaller Mn radius can be recognized from shorter bond lengths between NO/CH_3 and Mn (1.99 Å/2.04 Å), compared to the bond lengths by coordination with Rh atoms (2.04 Å/2.11 Å), respectively. For OH adsorption with binding energy of 0.24 eV stronger by replacing one Rh atom with Mn atom, the bond length between HO–Mn (2.04 Å) is smaller than HO–Rh bond (2.23 Å), accordingly.

In Table IV, molecules and radicals adsorption induced variations of work function are given. We find that for all molecular adsorptions at favorable sites, calculated work functions increase by 0.50 eV for N_2 (topRh), 0.99 eV for NO (hcpRh), and 1.42 eV for CO (hcpRh), respectively. These indicate a net charge transfer from the substrate to adsorbed molecules. In contrast, adsorption of OH and CH_3 radicals leads to a reduction of work function by 1.50 eV for OH at fccRhMn and 0.21 eV for CH_3 at topRh. Nevertheless, the differences of the variation of work function between different sites are modest except N_2, which is understandable because the energetics difference between different sites (ΔE_b in Table III) is largest for N_2.

IV. DISCUSSIONS

In the past, Mavrikakis *et al.* study the same set of adsorbates-Rh(111) by DFT.[29] Our results on Rh(111) agree, in general, with their work in terms of the order of adsorption energy and preference of adsorption sites for various species considered. However, as seen from Tables I and III, calculated energies show some difference in magnitude of about 0.20 eV, due to the different computational parameters used. In the present work, five layer slabs were used to model the metal surfaces, while three layer slabs were used in that work. We use Monkhorst-Pack $(6\times6\times1)$ grid, while 18 special k points in Ref. 29 on the same (2×2) unit cell. Moreover, RPBE was used self-consistently in the present work, instead of nonconsistent calculations there. We note that though RPBE is used self-consistently in the present work, the USPPs provided by DACAPO package are, however, generated within GGA Perdew-Wang formula (PW91). It is reported that changing the USPPs only causes the chemisorptions to be reduced by 30 meV and less than 10 meV for the two chemisorption systems, respectively.[30] Test calculations show that if we used the same parameters as used in Ref. 29, the results are exactly the same.

The above calculations show that RhMn(111) surface alloy with Mn presents distinct site selectivity and bond strength from Rh(111) surface. Except atomic oxygen and hydroxyls, all adsorbates on RhMn(111) surface alloy prefer to coordinate with Rh atoms (ensemble effects), and corresponding binding energies are 0.1–0.2 eV stronger than pure Rh(111) surfaces due to the ligand effects induced by Mn nearby. The strain effects induced by Mn is modest, as discussed below.

To illustrate the ligand effect induced by Mn, surface Rh 4d projected densities of states (PDOS) for both surfaces (without adsorbates) are plotted in Fig. 3. Compared to Rh(111) surface, 4d band of surface Rh atoms from RhMn(111) alloy surface is slightly narrowed, and the center of corresponding d band shifts upward from −2.03 to −1.96 eV. Meanwhile, a slight increase of PDOS at Fermi energy can be recognized. The upshift of d-band center and higher PDOS at Fermi energy would strength the interaction between adsorbates and substrates, according to Hammer-Norskov d-band theory.[45] We note that in RhMn(111) surface alloy, the distances between surface Rh atoms are 2.70 and

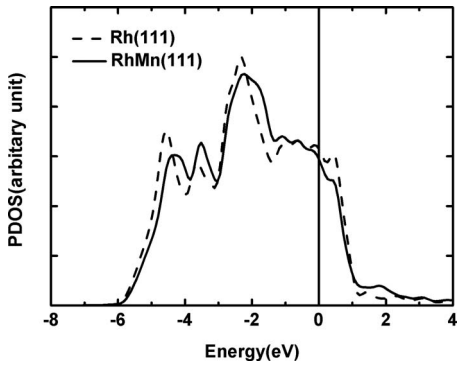

FIG. 3. Calculated projected density of states (PDOS) for surface Rh 4*d* orbital of bare RhMn(111) (solid line) and Rh(111) (dashed line) surfaces. The reference zero is Fermi energy indicated by the vertical line.

2.73 Å. Compared to that of clean Rh(111) (2.72 Å), the effect of strain (less than 1%) is expected to be modest.

The present DFT calculations show that atomic oxygen and hydroxyl group prefer to coordinate with Mn, instead of Rh. Calculated binding energies are lowered by 0.13 eV for O and 0.24 eV for OH when one adsorbates-Rh bond is replaced by one adsorbates-Mn bond. The stabilization comes from the enhanced hybridizations between O/OH and RhMn alloy surface, as supported by the electronic structure analysis. PDOS of oxygen and coordinated surface metal atoms at fccRhMn site and fccRh site are plotted in Figs. 4(a) and 4(b), respectively. For O adsorption at fccRh site with three O–Rh bonds, extensive hybridizations between O and Rh can be found at energy window of [−6.70 eV, −4.94 eV], which accounts for the overall binding between O and Rh underneath. For O adsorption at fccRhMn (two O–Rh bonds and one O–Mn bond), Fig. 4(a) shows that there is an overall upshift of PDOS, which would free some unfavorable antibonding states and stabilizes the interaction between O and RhMn substrates. Moreover, additional hybridization between O and Rh/Mn occurs at −4.40 eV, which strengthens the interaction between O and RhMn surface further. For other adsorbates such as carbon atom, as plotted in Fig. 4(c), similar hybridization as oxygen, however, cannot be found when carbon atom coordinates with Mn. Correspondingly, the site preference with Rh is maintained.

From the adsorption energies listed in Tables I and III, we find that for various species adsorbed on RhMn surface, the binding energy from the least to the most strongly bound species follows the order of $N_2 < CH_3 < CO < NO < H < OH < O < N < S < C$. Interestingly, the order of binding energies identified on RhMn surface alloy is exactly the same as the order of the adsorption on Rh(111) surface as found in the present work and that of Mavrikakis *et al.*[29] The ligand effect induced by Mn has little affect on the order of the binding energy of various species considered. The reason for this comes mainly from the dramatic different reactivity of these species, which varies from closed shell molecules with relative weak binding energy of −0.41 eV for N_2 to highly active open shell atoms with significantly strong binding to the metal substrates by −7.14 eV for carbon atom. This is in contrast to the Mn induced ligand effects and ensemble effects, which fall in the magnitude of 0.68 eV at

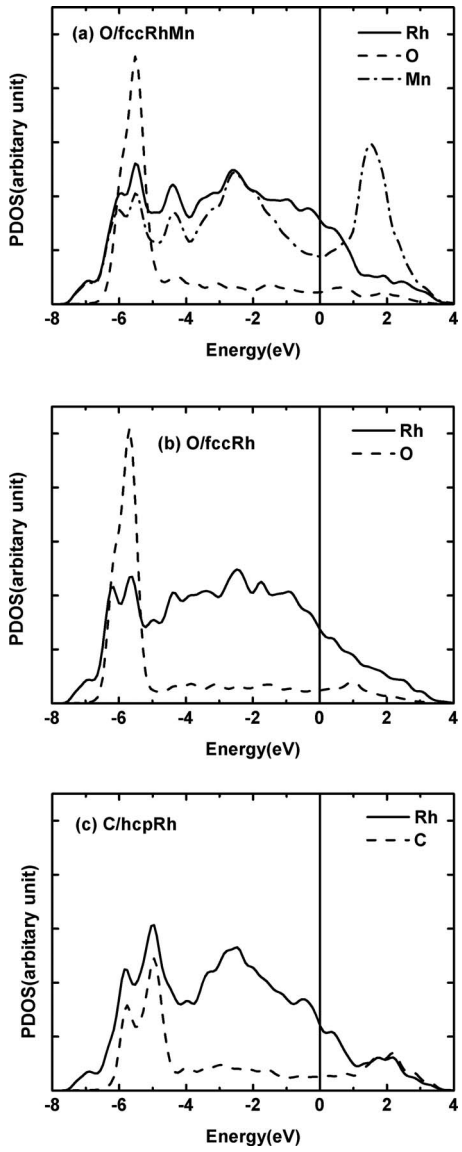

FIG. 4. Calculated projected density of states (PDOS) for adsorption of atomic oxygen (dashed line) at fccRhMn (a) and fccRh (b), and atomic carbon at hcpRh (c) on RhMn(111) surfaces. The PDOS of the coordinated metal atoms are represented by solid line for Rh and dashed-dotted line for Mn, respectively. The reference zero is Fermi energy indicated by the vertical lines.

maximum. For binucleus molecules N_2, CO, and NO with gradually increasing binding energy from −0.41 eV (topRh, N_2), to −1.87 eV (hcpRh, CO), and to −2.23 eV (hcpRh, NO), we note that N_2 is a closed shell homobinucleus molecule with little binding to the substrates. Though CO is a closed shell molecule either, its heterobinucleus nature and resulted redistribution of the electrons would allow pronounced hybridization with the substrates underneath and lead eventually to a stronger binding. For NO, it is clear that its open shell electronic configuration with one more extra electron than CO would enhance the binding further.

It is not surprising that the binding of the atomic species with respect to the metal substrate is much stronger than binuclear molecules due to the presence of large number of unpaired electrons, which would allow an extensive hybridization with *d* band of surface metal atoms. We note that

among various atomic species studied, the highest binding energy is approached for the adsorption of the atomic carbon. This can be rationalized from the difference of PDOS between carbon adsorption at hcpRh sites [Fig. 4(c)] and oxygen adsorption at fccRh site [Fig. 4(b)]. Compared to oxygen adsorption, the hybridizations between carbon and substrates underneath are more extensive first. Secondly, overall PDOS for the previous one is distributed at higher energy window, which would free more antibonding states to lower the energy of the system. These two together result in significantly stronger chemical bond formed between carbon and metal substrate than other atomic species or specifically atomic oxygen considered.

The site selectivity and modified bond strength of RhMn surface alloy are expected to have significant impact on the selectivity and reactivity, particularly for catalytic conversion of syngas (CO and H_2) from reforming of natural gas and coal to hydrocarbon (Fishcher-Tropsch synthesis) and oxygenates. In this context, we note that the selectivity and activity of alloy surfaces are sensitive to the reaction conditions. Calculated heat of formation of RhMn alloy shows that for pure RhMn alloy surface, Mn prefers to stay in the subsurface region, rather than embedded in the surface and bulk Rh layer. This configuration is energetically favorable under ultrahigh vacuum conditions, and probably hold true also under reducing conditions. However, under oxidizing conditions or with the presence of oxidic adsorbates such oxygen or hydroxyl group, their strong bonding with Mn may induce the segregation of Mn from the subsurface and surface alloys are developed. The formation of oxygen and hydroxyl group may come from the dissociation of CO and following hydrogenation under hydrogen rich conditions. Moreover, the hydroxyl group can be generated from the dissociation of water, which is present typically in the feed gas from the reforming processes.

In turn, the presence of Mn on the surface may facilitate the dissociation of CO and/or NO dissociation because of improved energetics, and the reactivity increases correspondingly. This is indeed found by experiments that the energy barrier for CO dissociation on RhMn catalysts is lower than on Rh catalysts.[46,47] Namely, the RhMn interfaces provide the active sites of CO dissociation. Since dissociated carbon atoms bond much strongly with Rh than Mn, the hydrogenation of carbon atoms to CH_x would take place in Rh domain. The preference of CH_3 coordination with Rh atoms indicates that Rh domain would be the active sites of C–C coupling for the growth of hydrocarbon chain. Adsorbed CO on Rh domain may react with CH_x to form oxygenates.

The present calculations indicate that RhMn and Rh catalysts for syngas conversion may suffer seriously the poison of sulfur due to its significantly strong binding with catalysts, compared to H_2 and CO adsorption as well as the activated dissociation of CO, which provides the source of carbon for the synthesis of hydrocarbon and oxygenates. Therefore, sulfur tolerant catalysts, which may be achieved by alloying with additional components, are desired. Tuning the relative activity between these elementary reaction steps and developing sulfur tolerant catalysts by varying the ratio of Rh and Mn (maybe third components) as well as their distributions are decisive for the selectivity of syngas conversion.

V. CONCLUSIONS

In the present work, density functional theory calculations have been employed to study atomic (H, C, N, O, S), molecular (N_2, NO, CO), and radical (CH_3, OH) adsorption on RhMn(111) alloy surfaces in terms of their energetics, preferential adsorption sites, as well as the underlying geometrical and electronic analysis. We find that Mn is energetically favorable to diffuse into the subsurface region under ultrahigh vacuum condition and/or reducing conditions. Under realistic conditions, the presence of the oxygen and hydroxyl group may induce Mn segregation from the subsurface region, and RhMn surface alloy is developed. On RhMn(111) surface alloy, we find that RhMn(111) surface alloy presents distinct activity and site selectivity with respect to Rh(111) surface. Independent of species considered (not including atomic oxygen and hydroxyl group), the interactions between these species and Rh atoms are preferential, and enhanced, in general, due to the ligand effects induced by Mn nearby. In contrast, oxygen-containing species (atomic oxygen and hydroxyl) prefer to coordinate with Mn atom due to the significant hybridization between oxygen and Mn, a manifestation of the ensemble effects. The identified order of the binding energies on RhMn alloy surface from the least to the most strongly bound is $N_2 < CH_3 < CO < NO < H < OH < O < N < S < C$, which is exactly the same as Rh(111) surface. The reason comes mainly from the distinct reactivity of these species varying from closed shell homonucleus molecule to atomic species with large number of unpaired electrons, which overwhelms the ligand/ensemble effects induced by alloy.

The modification of the adsorption energy and site preference on RhMn alloy surface found in the present work may have important implication on the syngas conversion. Regarding this, the activity and selectivity, which are decided by the reactants/intermediates selective and competitive adsorptions and balance between various elementary reaction steps required typically dual or multiple reaction centers, are concerned. Density functional theory calculations are helpful to shed new lights on this.

ACKNOWLEDGMENTS

We thank the National Natural Science Foundation of China (Nos. 20503030, 20873142, and 20733008) and Basic Research Program of China (No. 2007CB815205) for financial support.

[1] M. M. Bhasin, W. J. Bartley, P. C. Ellgen, and T. P. Wilson, J. Catal. **54**, 120 (1978).
[2] M. M. Bhasin and P. C. Ellgen, US Patent No. 4,096,164 (06/20/1978).
[3] A. G. T. M. Bastein, W. J. van der Boogert, G. van der Lee, H. Luo, B. Schuller, and V. Ponec, Appl. Catal. **29**, 243 (1987).
[4] S. C. Chuang, Jr., J. G. Goodwin, and I. Wender, J. Catal. **95**, 435 (1985).
[5] A. Kiennemann, R. Breault, J. P. Hindermann, and M. Laurin, J. Chem. Soc., Faraday Trans. 1 **83**, 2119 (1987).
[6] H. Y. Luo, W. Zhang, H. W. Zhou, S. Y. Huang, P. Z. Lin, Y. J. Ding, and L. W. Lin, Appl. Catal., A **214**, 161 (2001).

[7] B. J. Kip, P. A. T. Smeets, J. H. M. C. van Wolput, H. W. Zandbergen, J. van Grondelle, and R. Prins, Appl. Catal. **33**, 157 (1987).
[8] B. J. Kip, P. A. T. Smeets, J. van Grondelle, and R. Prins, Appl. Catal. **33**, 181 (1987).
[9] M. Ojeda, M. L. Granados, S. Rojas, P. Terreros, F. Javier Garcia-Garc, and J. L. G. Fierro, Appl. Catal., A **261**, 47 (2004).
[10] F. G. A. van der Berg, J. H. E. Glezer, and W. M. H. Sachtler, J. Catal. **93**, 340 (1985).
[11] K. P. de Jong, J. H. E. Glezer, H. P. C. E. Kuipers, A. Knoester, and C. A. Emeis, J. Catal. **124**, 520 (1990).
[12] H. Treviño and W. M. H. Sachtler, Catal. Lett. **27**, 251 (1994).
[13] H. Ma, Z. Yuan, Y. Wang, and X. Bao, Surf. Interface Anal. **32**, 224 (2001).
[14] H. Y. Luo, P. Z. Lin, S. B. Xie, H. W. Zhou, C. H. Xu, S. Y. Huang, L. W. Lin, D. B. Liang, P. L. Yin, and Q. Xin, J. Mol. Catal. A: Chem. **122**, 115 (1997).
[15] C. N. Satterfield, *Heterogeneous Catalysis in Industrial Practice*, 2nd ed. (Krieger, Malabar, 1996).
[16] V. K. Tzitzios, V. Georgakilas, and T. N. Angelidis, J. Chem. Technol. Biotechnol. **80**, 699 (2005).
[17] V. Ponec and W. M. H. Sachtler, J. Catal. **24**, 250 (1972).
[18] J. H. Sinfelt, J. L. Carter, and D. J. C. Yates, J. Catal. **24**, 283 (1972).
[19] V. Ponec, Appl. Catal., A **222**, 31 (2001).
[20] J. Schoiswohl, F. Mittendorfer, S. Surnev, M. G. Ramsey, J. N. Andersen, and F. P. Netzer, Phys. Rev. Lett. **97**, 126102 (2006).
[21] V. Stamenkovic, B. S. Mun, K. J. J. Mayrhofer, P. N. Ross, N. M. Markovic, J. Rossmeisl, J. Greeley, and J. K. Nørskov, Angew. Chem., Int. Ed. **45**, 2897 (2006).
[22] J. Kugai, S. Velu, and C. S. Song, Catal. Lett. **101**, 255 (2005).
[23] T. Ekou, A. Vicente, G. Lafaye, C. Especel, and P. Marecot, Appl. Catal., A **314**, 73 (2006).
[24] S. F. Zhang, Q. L. Qian, P. L. Pan, Y. Chen, G. Q. Yuan, Chin. Chem. Lett. **16**, 100 (2005).
[25] H. Y. Su, X. H. Bao, and W. X. Li, J. Chem. Phys. **128**, 194707 (2008).
[26] V. R. Stamenkovic, B. Fowler, B. S. Mun, G. F. Wang, P. N. Ross, C. A. Lucas, and N. M. Markovic, Science **315**, 493 (2007).
[27] Z. Paal, N. Gyorffy, A. Wootsch, L. Toth, I. Bakos, S. Szabo, U. Wild, and R. Schloegl, J. Catal. **250**, 254 (2007).
[28] J. Greeley and M. Mavrikakis, Catal. Today **111**, 52 (2006).
[29] M. Mavrikakis, J. Rempel, J. Greeley, L. B. Hansen, and J. K. Nørskov, J. Chem. Phys. **117**, 6737 (2002), and reference therein.
[30] B. Hammer, L. B. Hansen, and J. K. Nørskov, Phys. Rev. B **59**, 7413 (1999).
[31] D. Vanderbilt, Phys. Rev. B **41**, 7892 (1990).
[32] H. P. Singh, Acta Crystallogr., Sect. A: Cryst. Phys., Diffr., Theor. Gen. Crystallogr. **24**, 469 (1968).
[33] H. J. Monkhorst and J. D. Pack, Phys. Rev. B **13**, 5188 (1976).
[34] L. Bengtsson, Phys. Rev. B **59**, 12301 (1999).
[35] *CRC Handbook of Chemistry and Physics*, 76th ed. (CRC, New York, 1996).
[36] J. T. Yates, P. A. Thiel, and W. H. Weinberg, Surf. Sci. **84**, 427 (1979).
[37] W. A. Harrison, *Elementary Electronic Structure* (World Scientific Publishing Co. Pte. Ltd., Singapore, 1999).
[38] H. A. C. M. Hendrickx, A. Hoek, and B. E. Nieuwenhuys, Surf. Sci. **135**, 81 (1983).
[39] M. M. Yang, X. H. Bao, and W. X. Li, J. Chem. Phys. **127**, 024705 (2007).
[40] A. Beutler, E. Lundgren, R. Nyholm, J. N. Andersen, B. J. Setlik, and D. Heskett, Surf. Sci. **396**, 117 (1998).
[41] R. Linke, D. Curulla, M. J. P. Hopstaken, and J. W. Niemantsverdriet, J. Chem. Phys. **115**, 8209 (2001).
[42] D. Curulla, R. Linke, A. Clotet, J. M. Ricart, and J. W. Niemantsverdriet, Chem. Phys. Lett. **354**, 503 (2002).
[43] H. J. Borg, J. F. C. -J. M. Reijerse, R. A. van Santen, and J. W. Niemantsverdriet, J. Chem. Phys. **101**, 10052 (1994).
[44] V. P. Zhdanov and B. Kasemo, Catal. Lett. **40**, 197 (1996).
[45] B. Hammer and J. K. Nørskov, Surf. Sci. **343**, 211 (1995).
[46] W. M. H. Sachtler and M. Ichikawa, J. Phys. Chem. **90**, 4752 (1986).
[47] M. Ichikawa and T. Fukushima, J. Phys. Chem. **89**, 1564 (1985).